Near Rectilinear Halo Orbit Determination with Simulated DSN Observations

Nathan L. Parrish[1], Ethan Kayser[2], Matthew Bolliger[3],
Michael R. Thompson[4], Jeffrey S. Parker[5], Bradley W. Cheetham[6]
Advanced Space LLC, 2100 Central Ave, Boulder, CO 80301

Diane C. Davis[7]
ai solutions, 2224 Bay Area Blvd #415, Houston, TX 77058

Daniel J. Sweeney[8]
NASA JSC, 2101 E. NASA Pkwy, Houston, TX 77058

This paper presents the results of a high-fidelity simulation of spacecraft orbit determination in a near rectilinear halo orbit (NRHO). Others in the literature have examined this problem with linear covariance analysis,[9] but the highly-nonlinear dynamics of this orbit challenge the assumptions underlying such analyses. The present work builds on similar analysis performed by other authors[10] [11] [12] to contribute a fuller understanding of the operational requirements for NRHO navigation. The present work serves as a check to the assumptions of previous studies and an independent verification of those results. The results from the literature are extended by quantifying the space of orbital states from which a spacecraft with given control authority can safely return to the nominal path. Spacecraft state uncertainty estimates are evaluated as a function of time. Simulated range and range-rate measurements with the Deep Space Network (DSN) ground stations are used to model orbit determination accuracy. Orbit maintenance maneuvers are performed using both short-horizon and long-horizon stationkeeping targeting. Monte Carlo analysis of orbit determination and stationkeeping is performed.

This paper quantifies the achievable state uncertainty with deep space network (DSN)-only range and range-rate observations. This paper also addresses requirements on the frequency of DSN observation periods and correlates ground contact frequency with navigation accuracy. The results of several related studies are presented and discussed: the effect of missing ground station passes, the effect of missing stationkeeping maneuvers, the sensitivity of the spacecraft state estimate to realistic error sources, and stationkeeping propellant budget.

[1] Optimization Lead, Advanced Space, LLC, 2100 Central Ave STE 102, Boulder, CO 80301. AIAA member.
[2] Aerospace Engineer, Advanced Space, LLC, 2100 Central Ave STE 102, Boulder, CO 80301. AIAA member.
[3] Aerospace Engineer, Advanced Space, LLC, 2100 Central Ave STE 102, Boulder, CO 80301. AIAA member.
[4] Aerospace Engineer, Advanced Space, LLC, 2100 Central Ave STE 102, Boulder, CO 80301. AIAA member.
[5] Chief Technology Officer, Advanced Space, LLC, 2100 Central Ave STE 102, Boulder, CO 80301. AIAA member.
[6] Chief Executive Officer, Advanced Space, LLC, 2100 Central Ave STE 102, Boulder, CO 80301. AIAA member.
[7] Principal Systems Engineer, ai solutions, 2224 Bay Area Blvd #415, Houston TX 77058.
[8] Gateway Integrated Spacecraft Performance Lead, NASA Johnson Space Center, 2101 E. NASA Pkwy, Houston, TX 77058.
[9] C. Newman et al., "Stationkeeping, Orbit Determination, and Attitude Control for Spacecraft in Near Rectilinear Halo Orbits", Proceedings of the AAS/AIAA Astrodynamics Specialists Conference, Paper AAS 18-388, Snowbird, UT, 19-23 August 2018.
[10] C. Newman et al., "Attitude Control and Orbit Determination of a Crewed Spacecraft with Lunar Lander in Near Rectilinear Halo Orbit", Proceedings of the AAS/AIAA Space Flight Mechanics Meeting, Paper AAS 19-545, Ka'anapali, HI, 13-17 January 2019.
[11] M. Volle, "Distant Retrograde Orbit Constellations for Relative-Only Navigation in Near Rectilinear Halo Orbits", Proceedings of the AAS/AIAA Space Flight Mechanics Meeting, Paper AAS 19-551, Ka'anapali, HI, 13-17 January 2019.
[12] M. Volle and D. Davis, "Examining the Feasibility of Relative-Only Navigation for Crewed Missions to Near Rectilinear Halo Orbits", Paper AAS 18-351.

I. Introduction

NASA's current plans for human and robotic exploration include a renewed focus on the Moon. Two upcoming missions, the crew-tended Gateway and the robotic Capstone spacecraft, plan to exploit low-cost mission opportunities offered by multibody orbits. Both spacecraft plan to primarily reside in Near Rectilinear Halo Orbits (NRHOs) near the Moon. Nearly stable members of the halo orbit families, southern L_2 NRHOs are inexpensive to maintain, and they offer extensive coverage of the lunar south pole, fast and relatively inexpensive access to the lunar surface, and favorable aborts back to the Earth.[13] To achieve inexpensive orbit maintenance, safe rendezvous, and reliable disposal of spacecraft from NRHO, accurate orbit determination (OD) within the NRHO is required.

Many missions, including ICEE-3, Genesis, ACE, SOHO and Wind,[14] have successfully operated in Sun-Earth halo orbits. The upcoming JWST and WFIRST[15] missions are also planned to reside in Sun-Earth halos. A single mission to date, the 2010 ARTEMIS mission that served as an end-of-life opportunity for two of the THEMIS spacecraft, has demonstrated successful operations, including accurate OD, in Earth-Moon halo orbits.[16] The CAPSTONE mission, scheduled to launch in December 2020, and the Gateway starting in 2022 will be the first spacecraft to operate in NRHOs.

NRHOs represent a subset of the L_1 and L_2 halo orbits, bounded by changes in linear stability. Some NRHOs are linearly stable in the Earth-Moon circular restricted three-body dynamics; others are slightly unstable. The current nominal orbit for the Gateway is a 9:2 synodic resonant southern L_2 NRHO, meaning that the spacecraft completes 9 revolutions about the Moon for every 2 synodic revolutions of the Moon about the Earth. This resonance is favorable because it minimizes the amount of time spent in the Earth's shadow while offering favorable lunar surface access. NRHOs with a 9:2 resonance are linearly unstable. However, small maneuvers can maintain a safe orbit for a ΔV cost on the order of a few meters per second per year. A 9:2 resonant NRHO appears in the Earth-Moon rotating frame Figure 1a.

Certain characteristics of NRHOs complicate orbit determination. For example, when propagated in a high fidelity ephemeris model, an NRHO is quasi-periodic in the Earth-Moon rotating frame, and the orbital plane is approximately perpendicular to the line-of-sight from Earth. This geometry leads to navigational challenges, since Earth-based range and range-rate measurements cannot directly measure the orbital motion; the system is poorly observable. Additionally, NRHOs are characterized by large variations in the distance to the Moon; the radius of the 9:2 NRHO ranges from approximately 3,500 km at perilune to about 71,000 km at apolune. These significant differences cause the acceleration experienced by the spacecraft to vary by 2-3 orders of magnitude within a single revolution. The variation in acceleration experienced by a spacecraft in an NRHO is compared to the variation in acceleration experienced by a spacecraft in low lunar orbit (LLO) in Figure 1b. This extreme change in dynamics is comparable (in terms of navigational challenge) to performing a lunar flyby once every week.

Further navigational complications arise from the limited control authority available to a spacecraft with solar electric propulsion (SEP), such as the Power and Propulsion Element (PPE) of the Gateway. It is apparent in Figure 1b that the SEP control acceleration is considerably less than the gravity of the Moon and Earth at all times. If the orbit determination filter fails to track the spacecraft, there is a potential risk that the spacecraft's path could diverge beyond the point of recoverability by the SEP thrusters. That is, there is some amount of spacecraft state error beyond which the spacecraft's limited control authority is inadequate to return to the nominal NRHO without large corrections or the use of an alternative propulsion system such as RCS thrusters.

[13] R. Whitley and R. Martinez, "Options for Staging Orbits in Cislunar Space," IEEE Aerospace Conference, Big Sky, Montana, March 2016.

[14] D. W. Dunham and R. W. Farquhar, "Libration Point Missions 1978-2002," Libration Point.

[15] N. Bosanac, C. M. Webster, K. C. Howell, and D. C. Folta, "Trajectory Design and Stationkeeping Analysis for the Wide Field Infrared Survey Telescope Mission," AAS/AIAA Astrodynamics Specialists Conference, Long Beach, California, August 2017.

[16] M. Woodard, D. Cosgrove, P. Morinelli, J. Marchese, B. Owens, and D. Folta, "Orbit determination of spacecraft in Earth-Moon L1 and L2 libration point orbits," AAS/AIAA Astrodynamics Specialists Conference, Girdwood, Alaska, August 2011.

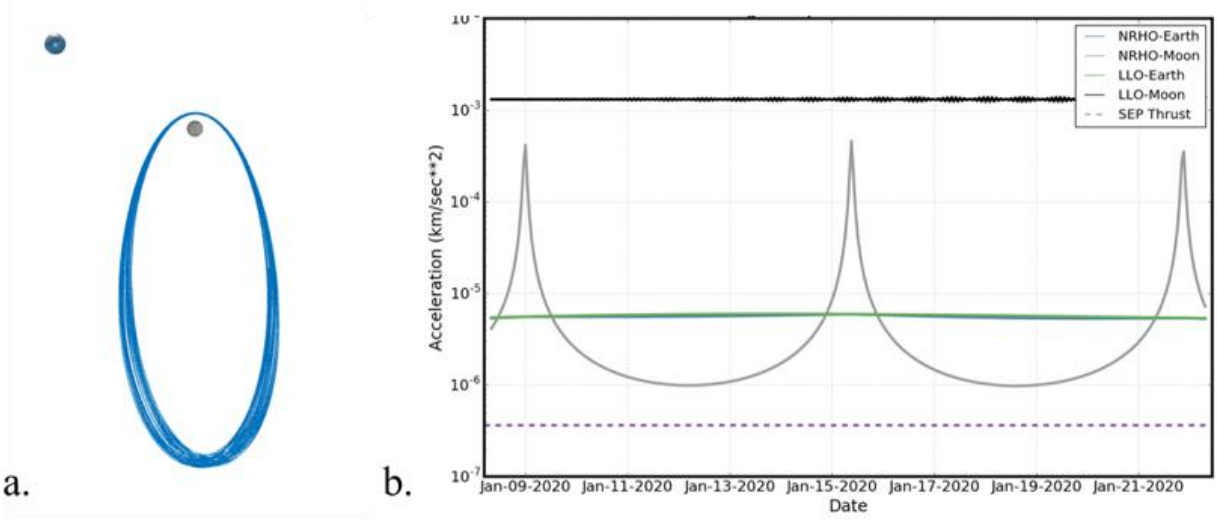

Figure 1. 9:2 NRHO in the Earth-Moon rotating frame (a); Accelerations acting on spacecraft in LLO and NRHO orbits (b).

Several investigations have already begun to explore orbit determination in the lunar NRHO regime. Newman et al.[17] perform a linear covariance analysis as a first look at NRHO navigation with Deep Space Network (DSN) tracking. Winternitz et al.[18] explore the enhancement in the OD solution available when a GPS receiver is included onboard, and Yun et al.[19] investigate adding optical measurements as well. Guinn et al.[20] investigate relative-only optical navigation strategies. Since the highly-nonlinear dynamics of this orbit challenge the assumptions underlying linear covariance analyses, further analyses by Newman et al.[21] and Volle et al.[22, 23] employ Monte Carlo OD simulations using both DSN and relative measurements.

The present work serves as a check to the assumptions of previous studies and an independent verification of those results. The results from the literature are extended by quantifying the space of orbital states from which a spacecraft with given control authority can safely return to the nominal path. Spacecraft state uncertainty estimates are evaluated as a function of time. Simulated range and range-rate measurements with DSN ground stations are used to model orbit determination accuracy. Orbit maintenance maneuvers are performed using both short-horizon and long-horizon stationkeeping targeting. Finally, Monte Carlo analysis of orbit determination and stationkeeping is performed.

[17] C. Newman et al., "Stationkeeping, Orbit Determination, and Attitude Control for Spacecraft in Near Rectilinear Halo Orbits", Proceedings of the AAS/AIAA Astrodynamics Specialists Conference, Paper AAS 18-388, Snowbird, UT, 19-23 August 2018.

[18] L. B. Winternitz, W. A. Bamford, A. C. Long, and M Hassouneh, "GPS Based Autonomous Navigation Study for the Lunar Gateway," AAS Guidance, Navigation, and Control Conference, Breckenridge, Colorado, February 2019.

[19] S. Yun, K Tuggle, R. Zanetti, and C. D'Souza, "Sensor Configuration Trade Study for Navigation in Near Rectilinear Halo Orbits," AAS/AIAA Astrodynamics Specialists Conference, Portland, Maine, August 2019.

[20] J. R. Guinn, S. Bhaskaran, T. A. Ely, B. M. Kennedy, T. J. Martin-Mur, R. S. Park, J. E. Riedel, D. C. Roth, and A. T. Vaughan, "The Deep Space Positioning System (DPS) Navigator Concept for the Lunar Gateway," 42nd Annual AAS Guidance and Control Conference, Breckenridge, Colorado, February 2019.

[21] C. Newman et al., "Attitude Control and Orbit Determination of a Crewed Spacecraft with Lunar Lander in Near Rectilinear Halo Orbit", Proceedings of the AAS/AIAA Space Flight Mechanics Meeting, Paper AAS 19-545, Ka'anapali, HI, 13-17 January 2019.

[22] M. Volle, "Distant Retrograde Orbit Constellations for Relative-Only Navigation in Near Rectilinear Halo Orbits", Proceedings of the AAS/AIAA Space Flight Mechanics Meeting, Paper AAS 19-551, Ka'anapali, HI, 13-17 January 2019.

[23] M. Volle and D. Davis, "Examining the Feasibility of Relative-Only Navigation for Crewed Missions to Near Rectilinear Halo Orbits", Paper AAS 18-351.

II. Dynamics and Assumptions

Spacecraft dynamics are modeled in GMAT (the General Mission Analysis Tool, developed at Goddard Space Flight Center) [reference] and Monte (Mission Analysis, Operations, and Navigation Toolkit Environment, developed at the Jet Propulsion Laboratory) [reference]. In this analysis, GMAT generates the "truth" solution with the following forces modeled:

- 32x32 spherical harmonics gravity field model of the Moon from the GRGM 900c model.
- Point masses of the Earth, Sun, and barycenters of all other planetary systems in the solar system, with states from the JPL DE430 ephemerides.[24]
- Solar radiation pressure (SRP) with a spherical spacecraft with coefficient of reflectivity of 1.3. Mass and surface area depend on the Gateway configuration according to Table 1. These values are representative of possible Gateway configurations.
- Relativistic correction.

The filter dynamics are slightly different from the "true" dynamics in order to represent realistic mis-modeling of small forces. Note that although the spherical model for SRP is not generally very accurate, it is a good approximation in this case. The Gateway is assumed to be oriented in SPEA (solar pressure equilibrium attitude), a fixed attitude identified to minimize torques caused by SRP. Since this attitude is fixed relative to the Sun, using an equivalent area flat plate or spherical model captures the true dynamics accurately. The filter dynamics are implemented separately in GMAT and Monte and include the following forces:

- 8x8 spherical harmonics gravity field model of the Moon from the GRGM 900c model.
- Point masses of the Earth, Sun, and barycenters of all other planetary systems in the solar system, with states from the JPL DE430 ephemerides.[25]
- Solar radiation pressure with a spherical spacecraft. Mass, surface area, and coefficient of reflectivity are initialized randomly with error according to the uncertainties given in Table 2.
- No relativistic correction.

Navigation is simulated separately in GMAT and in Monte. In both navigation simulations, the filter defines the dynamics in an Earth-centered J2000 inertial reference frame.

The GMAT simulation uses a batch filter iterated until convergence. Convergence is defined as meeting the absolute and relative weighted RMS convergence criteria (0.01 and 0.001, respectively) and usually takes 3-5 iterations. GMAT's outer loop sigma editing (OLSE) is not used here because the simulated measurements are known to all be valid. In real operations, outlier measurements would be ignored to avoid incorporating bad data.

The Monte simulation compares two different filters: the U-D factorized covariance filter, and the square root information filter (SRIF). The Monte filter uses stochastic accelerations on the order of 5×10^{-7} mm/s^2 updated every 8 hours to absorb dynamical mis-modeling.

In this analysis, a data arc always consists of nearly one complete orbit, starting immediately after the orbit maintenance maneuver (OMM) performed at apolune, and ending at the data cutoff 24 hours before the next apolune. Ground station tracking passes are allowed between apolune and data cutoff. OMMs are not estimated. Future analysis will model the OMMs in the filter and also allow tracking passes during the 24 hours between data cutoff and the next apolune (these data would be used to estimate the state for the subsequent data cutoff).

All analyses in this paper use three DSN (deep space network) ground stations, with a maximum of one ground station active at a time. The ground stations simulate a 35-m dish at the Madrid, Canberra, and Goldstone facilities. The Gateway is assumed to communicate with the DSN on X-band radio. Measurement noise in reality is dependent on many factors, such as the ground radio specifications, spacecraft radio specifications, and weather in Earth's ionosphere [reference]. The measurement noise specified in Table 2 is chosen to be similar to the real measurement noise found from post-processing of the ARTEMIS mission.[26]

[24] Folkner, W. M., Williams, J. G., Boggs, D. H., Park, R. S. & Kuchynka, P. *The Planetary and Lunar Ephemerides DE430 and DE431*. *Interplanet. Netw. Prog. Rep* 196, (2014).

[25] Folkner, W. M., Williams, J. G., Boggs, D. H., Park, R. S. & Kuchynka, P. *The Planetary and Lunar Ephemerides DE430 and DE431*. *Interplanet. Netw. Prog. Rep* 196, (2014).

[26] Leonard, J. M., Cheetham, B. W., and Born, G. H. Preliminary Evaluation of Earth-Moon Libration Point Orbit Navigation with Post-Processed ARTEMIS Data. 2014.

All maneuvers are assumed to be impulsive changes in velocity (ΔV). Launch is not modeled. The simulation begins in a 100 km circular parking orbit around Earth with inclination of 28.5º, approximating the condition immediately after launch from Kennedy Space Center.

As the Gateway is constructed element-by-element, there will be many different vehicle configurations, each with its own operational requirements. In the present analysis, only the first two potential configurations are examined: PPE (power & propulsion element) only, and PPE + HALO. In these configurations, Gateway is in a quiescent (uncrewed) state, which results in smaller perturbations. With crew aboard, venting becomes a significant source of uncertainty in the dynamics. Later configurations also experience larger gravity gradient torques near perilune, requiring more frequent momentum wheel desaturation maneuvers. The present analysis assumes that a single desaturation maneuver is performed each orbit in a random direction, immediately before each OMM.

Table 1. Gateway configurations analyzed.

Gateway Configuration	*Mass [kg]*	*Sun-facing area [m^2]*
1) PPE	5700	310
2) PPE + HALO	13700	340

Table 2. Assumed sources of uncertainty.

Error source	*Uncertainty (3-sigma)*
Mass uncertainty	3%
SRP area	30%
Coefficient of reflectivity	45%
OMM execution error	1.42 mm/s fixed, 1.5% proportional, 1 deg pointing
Measurement bias	7.5 m (range), 2.5 mm/s (range-rate)
Measurement noise	3 m (range), 1 mm/s (range-rate)

Table 3. A priori state error and covariance.

Estimated parameter	*3σ a priori state error relative to truth (applied once at start of simulation)*	*a priori covariance (re-initialized at the start of every data arc)*
Position in Earth-centered J2000	10 km	∞ km
Velocity in Earth-centered J2000	10 cm/s	∞ m/s
Coefficient of reflectivity	45%	∞
Range measurement bias	1 m	∞
Range-rate measurement bias	0.35 mm/s	∞

III. Navigation Study Setup

The present work builds on similar analysis performed by other authors[27, 28, 29] to contribute a fuller understanding of the operational requirements for NRHO navigation. Typical statistical orbit determination relies on two fundamental assumptions:

1) The spacecraft state uncertainty distribution is always Gaussian.
2) The state dynamics and measurement-state relationships can be linearized relative to a reference trajectory.

In an NRHO, both of these assumptions are pushed to their limits. Figure 2 shows how the standard moments (standard deviation, skewness, and excess kurtosis) evolve over time, for an initial 3σ covariance of 10 km position in each axis and 10 cm/s velocity in each axis. The values in Figure 2 are computed based on a Monte Carlo simulation with 1,000 samples. Even over a single orbit, the dynamics are clearly nonlinear, and the state uncertainty quickly becomes non-Gaussian.

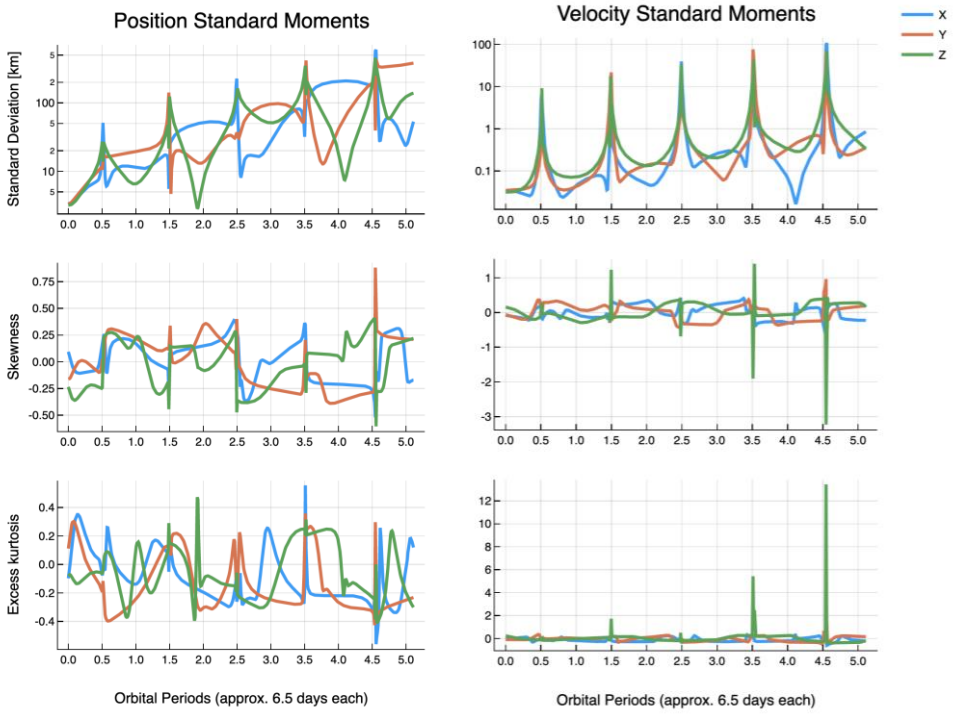

Figure 2. Evolution of position and velocity standard moments over time in an NRHO.

Linear covariance analysis is a common way to approximate spacecraft navigation performance. A covariance analysis, also known as a Cramer-Rao analysis, is essentially equivalent to a single iteration of a sequential filter. The update to the covariance matrix is computed with each measurement, but the measurement is not used to update the state estimate. Covariance analysis is adequate when the fundamental assumptions described above are satisfied or nearly satisfied. However, covariance analysis on its own can be misleading. For instance, it is entirely possible that a navigation filter would saturate and converge on an incorrect solution. Stochastic acceleration may be required in a real filter to capture significant but difficult-to-model small forces. Engineering intuition is required to ensure that the covariance analysis does not return overly-optimistic results. Given the highly-nonlinear dynamics in an NRHO, it is not immediately obvious to what extent linear covariance analysis can be trusted in this regime. The goal of the present

[27] C. Newman et al., "Attitude Control and Orbit Determination of a Crewed Spacecraft with Lunar Lander in Near Rectilinear Halo Orbit", Proceedings of the AAS/AIAA Space Flight Mechanics Meeting, Paper AAS 19-545, Ka'anapali, HI, 13-17 January 2019.
[28] M. Volle, "Distant Retrograde Orbit Constellations for Relative-Only Navigation in Near Rectilinear Halo Orbits", Proceedings of the AAS/AIAA Space Flight Mechanics Meeting, Paper AAS 19-551, Ka'anapali, HI, 13-17 January 2019.
[29] M. Volle and D. Davis, "Examining the Feasibility of Relative-Only Navigation for Crewed Missions to Near Rectilinear Halo Orbits", Paper AAS 18-351.

analysis is to set up a realistic navigation analysis which makes the fewest assumptions possible, then quantify the navigation performance for various operations parameters.

The navigation simulation uses three spacecraft: the Reference, which is an idealized target; the Truth, which simulates the real spacecraft; and the Navigation spacecraft, which represents the best estimate of the Truth at any time. Figure 3 illustrates the role each of these spacecraft play in the simulation. The filter never knows the state of the Truth directly. Simulated range and range-rate measurements are generated (with noise and bias errors) from the Truth and subsequently passed through the filter, as shown in Figure 4.

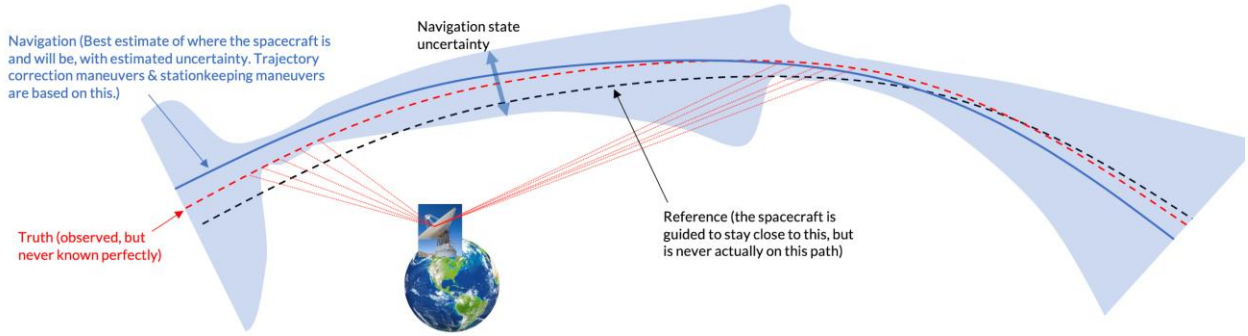

Figure 3. Conceptual diagram of the relationship between the Reference, Navigation, and Truth spacecraft.

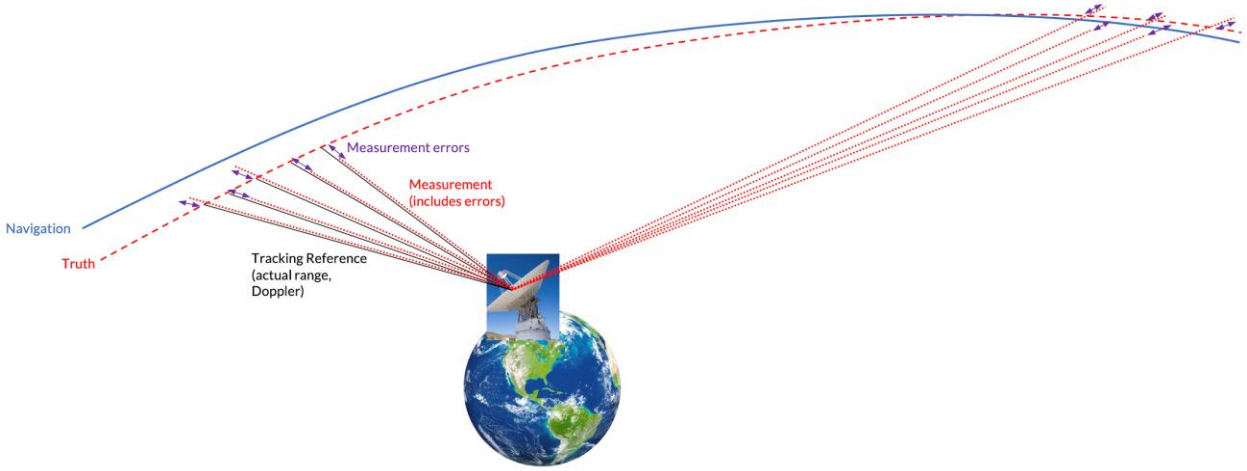

Figure 4. Conceptual diagram of measurement errors.

In multi-body dynamics, results in the literature have shown that the navigation state accuracy is closely correlated to mission ΔV.[30] The present results agree with that finding. Figure 5 shows a conceptual diagram of why that is the case. Trajectory correction maneuvers (TCMs) or stationkeeping (SK) maneuvers are always designed based on the Navigation spacecraft — the best estimate of the Truth state. In general, there will always be some error between the Navigation state and the Truth state at the maneuver execution epoch. This error is exacerbated by a simple practical concern: the maneuver must be designed based on data available as of the data cutoff epoch, which is typically 1-3 days before the maneuver execution epoch for deep space missions. Between the data cutoff epoch and the maneuver execution epoch, the ground-based navigation team must carry out a series of important analyses: process the measurement data to-date, design a nominal maneuver, ensure that the maneuver execution error will not endanger

[30] K.C. Howell and S.C. Gordon. Orbit determination error analysis and a station–keeping strategy for Sun–Earth L1 libration point orbits. Journal of the Astronautical Sciences, 42:207–228, 1994.

the mission, build the spacecraft instructions, and upload the instructions to the spacecraft. A good example of this process is described in the experience from the Dawn mission[31].

While these ground-based operations are taking place, the Navigation state uncertainty grows. When the maneuver is executed, it is based on an incorrect state estimate and executed with error. If these errors are small, they do not contribute much to the total ΔV of the mission. However, the chaotic nature of multi-body dynamics means that real errors have a significant effect on the mission. In a navigation simulation, care must be given to represent these constraints and errors realistically.

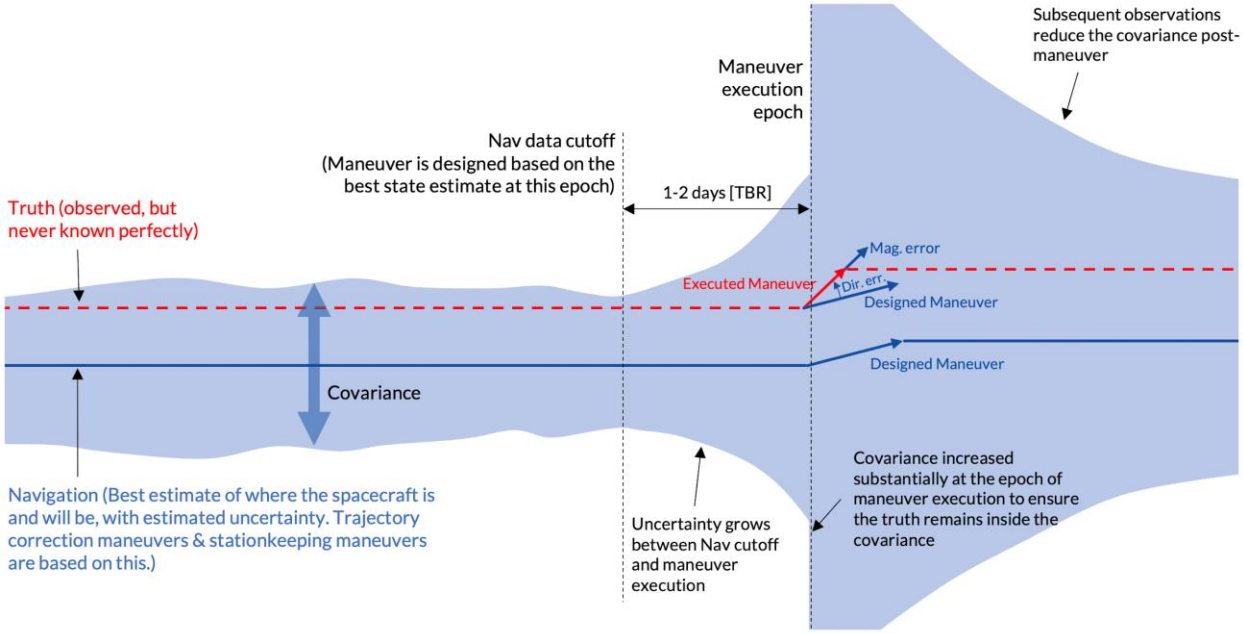

Figure 5. Conceptual diagram of navigation errors and uncertainty.

In order to preserve the validity of the results of a simulated navigation study, it is important that the navigation estimate never directly touches the truth. Or, in other words, the navigation simulation must not cheat by having unrealistic knowledge of the truth. This concept is visualized in Figure 6. The present analysis goes to lengths to ensure that the Truth and Navigation spacecraft are isolated from each other. This is done by modeling them in different software (Truth in GMAT or Copernicus, Navigation in Monte), using different force models, and using realistic a priori state error and covariance in the filter.

[31] Han, D. "Orbit Transfers for Dawn's Vesta Operations: Navigation and Mission Design Experience." *23rd International Symposium on Space Flight Dynamics*, No. February 2009, 2012, pp. 1–15.

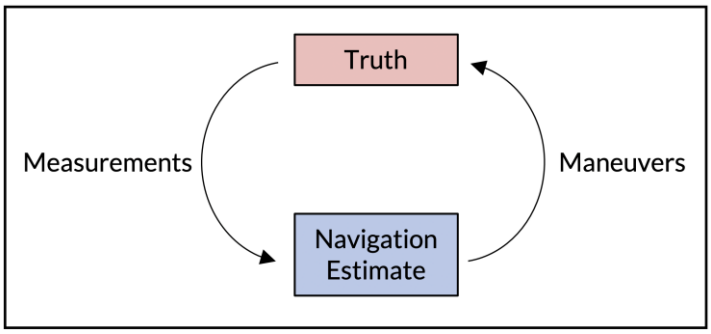

Figure 6. Conceptual relationship between truth and the navigation estimate.

One common metric for filter performance is the covariance at the end of a data arc. However, as noted above, the covariance alone is not a sufficient metric. In the present analysis, filter performance is judged based on the following characteristics, in addition to the covariance:

- Convergence or divergence.
- Truth trajectory remaining within the uncertainty bounds of the navigation solution.
- Accuracy of the navigation solution (relative to truth).
- The ability of the truth spacecraft to efficiently and safely maintain its orbit while executing maneuvers designed based on the navigation solution.

IV. Results

The results in this section describe analyses of NRHO insertion cleanup, stationkeeping with simulated orbit determination, and navigation trades.

A. NRHO Insertion

Because the NIM is modeled to occur at perilune, an area known to be very dynamically sensitive, a pair of post-insertion maneuvers is designed to bring the resulting trajectory closer to the reference. The strategy for these maneuvers is based off of the long-horizon orbit maintenance strategy described in Davis et al.[32] The Insertion Correction Maneuver (ICM) strategy is depicted in Figure 7. ICM-1 targets the position of the reference orbit at the epoch of ICM-2. After ICM-1 is performed, the spacecraft coasts to ICM-2, where it targets velocity continuity with the reference at the same epoch. This maneuver is not applied, however, and instead is used as the initial guess for an OMM, which is performed in place of ICM-2. The standard OMM procedure is described in Section IV B.

[32] Davis, D. C., F. Khoury, and K. C. Howell, "Phase Control and Eclipse Avoidance in Near Rectilinear Halo Orbits," 43rd AAS Guidance, Navigation and Control Conference, Breckenridge, Colorado, February 2020.

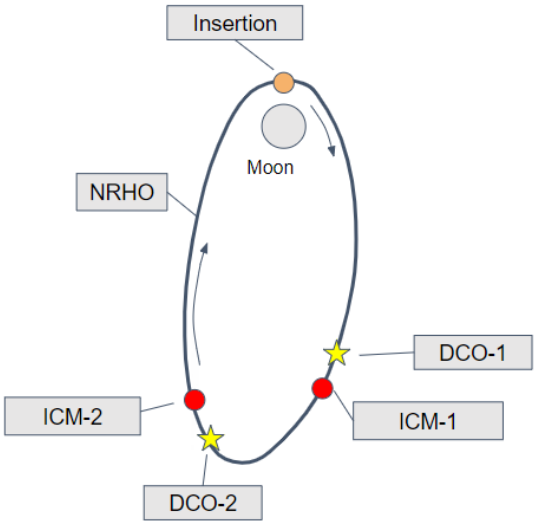

Figure 7. Conceptual diagram of the Insertion Correction Maneuvers strategy.

For this analysis, it is assumed that there is continuous tracking between insertion and the first data cutoff point, labelled DCO-1 in Figure 7, as well as between ICM-1 and DCO-2. Trades in the elapsed time between each of DCO points and maneuver execution times, the temporal spacing of the maneuvers, and the insertion errors are all considered. The insertion errors are summarized in Table 4, and the trades are summarized in Table 5. Each case in Table 6 represents a Monte Carlo analysis of approximately 100 runs, each sampling random errors for insertion, desaturation perturbations, and OMM execution. The distribution of insertion errors was determined by sampling errors for trajectory correction maneuvers (TCMs) for a ballistic lunar transfer (BLT) leading to an NRHO. The navigation requirements and expected performance are studied in a parallel analysis in Parrish et al.[33]

Table 4. Summary of 1-sigma insertion errors.

Case	X [km]	Y [km]	Z [km]	VX [m/s]	VY [m/s]	VZ [m/s]
High	10	10	10	5	5	5
Low	1	1	1	0.5	0.5	0.5

Table 5. Summary of Insertion Correction Maneuver trades.

Case	Time between insertion and DCO-1	Time between DCO-1 and ICM-1	Time between ICM-1 and DCO-2	Time between DCO-2 and ICM-2	Insertion Errors
1	2 days	8 hours	2 days	1 day	High
2	2 days	8 hours	2 days	1 day	Low
3	1 day	8 hours	2.5 days	1 day	High

[33] Parrish, N. L., Kayser, E., Bolliger, M., Thompson, M.R., Parker, J.S., Cheetham, B.W., Davis, D.C., "Ballistic Lunar Transfers to Near Rectilinear Halo Orbit: Operational Considerations", in *AIAA/AAS Spaceflight Mechanics Conference*, Orlando, 2020.

4	1 day	8 hours	2.5 days	1 day	Low
5	1 day	1 day	2 days	1.5 days	High
6	1 days	1 day	2 days	1.5 days	Low

The results for each case are presented in Table 6. In all cases, ICM-1 contributes most of the total DV cost. In general, a higher insertion perturbation corresponds to a higher total ICM cost. Further, the greater the separation between ICM-1 and ICM-2, the lower the total cost. This is expected, as the greater time span allows for a larger lever arm between the maneuvers.

Table 6. Summary of ICM results.

Case	ICM-1 Cost [m/s]	ICM-2 Cost [m/s]	Total ICM Cost [m/s]
1	TBD	TBD	TBD
2	TBD	TBD	TBD
3	TBD	TBD	TBD
4	TBD	TBD	TBD
5	TBD	TBD	TBD
6	TBD	TBD	TBD

B. Stationkeeping

This analysis implements both a short-horizon and a long-horizon stationkeeping strategy, with state estimation updates provided by a navigation filter processing simulated observations. The short-horizon algorithm is designed to keep the spacecraft in the vicinity of the NRHO without applying stringent, expensive constraints. The long-horizon strategy is applied to maintain the phase of the NRHO; that is, to ensure the perilune passage time of the Gateway does not drift far from that of the reference NRHO. The goal is to avoid long eclipses from the Earth's shadow, which are absent from the reference,[34] and also to provide a predictable state for spacecraft arriving and departing from the Gateway. The predictable timing of the Gateway state within the NRHO will facilitate transfers to and from Earth as well as lander missions to the lunar surface.

The short-horizon stationkeeping strategy implemented in the current study is an x-axis crossing control scheme. A maneuver at apolune is designed to target the x-component of rotating velocity, v_x, along a reference trajectory at perilune 6.5 revolutions downstream. This strategy has been found effective in the literature.[35,36] OMMs with magnitudes under 3 cm/s are not executed for the sake of operational simplicity.

[34] Lee, D. "Gateway Destination Orbit Model: A Continuous 15 Year NRHO Reference Trajectory," NASA Technical Report, August 2019.

[35] Davis, D. C. *et al.* Orbit Maintenance and Navigation of Human Spacecraft at Cislunar Near Rectilinear Halo Orbits. in *27th AAS/AIAA Space Flight Mechanics Meeting* (2017).

[36] Newman, C. P., Sieling, R., Davis, D. C. & Whitley, R. J. Attitude Control and Orbit Determination of a Crewed Spacecraft With Lunar Lander in Near Rectilinear Halo Orbit. *AAS Astrodyn. Spec. Conf.* 1–19 (2019).

This analysis implements an alternative long-horizon stationkeeping strategy, depicted in Figure 8. The strategy is similar to that of Davis et al.[37] with some minor modifications, most notably with regard to the timing of the maneuvers along the orbit: both of the long-horizon maneuvers are performed at apolune. The first maneuver, which occurs at time t_0, targets the position vector and the apolune epoch of the reference NRHO one revolution downstream, at time t_1. The resulting post-maneuver state is propagated for one revolution, to t_1, at which time the second long-horizon maneuver is designed. This second maneuver simply achieves velocity continuity with the reference at apolune.

At this stage there are two feasible options. The first option performs the second maneuver as designed (subject to maneuver execution errors). The second option does not perform that maneuver, but instead uses it as the initial guess for an OMM that occurs at apolune, according to the short-horizon stationkeeping strategy. Both options are effective strategies for long-term maintenance of the NRHO, as both implementations are found to safely maintain the NRHO for at least one year. However, the first option achieves an orbit that is closer to the reference, as it targets the full 7-state. Because of these extra constraints, though, this option results in more expensive long-horizon maneuvers than the second option. It is possible that the first option, though more expensive, may prove necessary for multi-year stationkeeping. A comparison of these strategies is presented in Table 9.

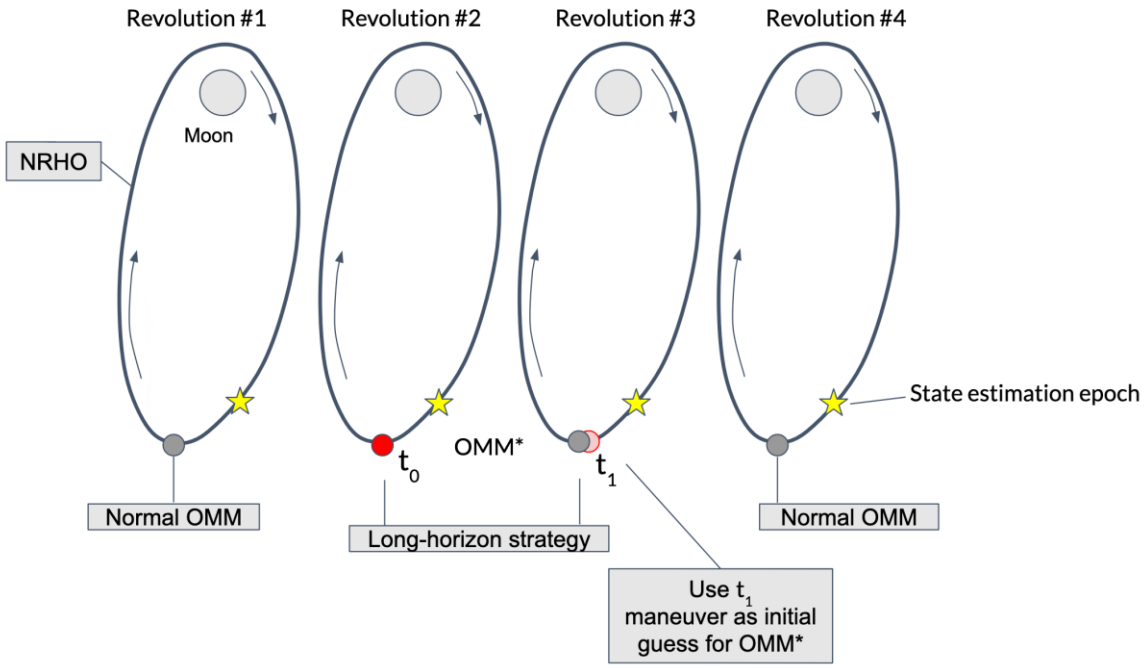

Figure 8. Conceptual diagram of the apolune-to-apolune long-horizon stationkeeping strategy.

[37] Davis, D. C., F. Khoury, and K. C. Howell, "Phase Control and Eclipse Avoidance in Near Rectilinear Halo Orbits," 43rd AAS Guidance, Navigation and Control Conference, Breckenridge, Colorado, February 2020.

Table 7. Results of Monte Carlo trials of apolune-to-apolune stationkeeping strategy. *Cases 1 & 2 use a batch filter on simulated range and range-rate data. Cases 3-6 approximate navigation by perturbing the "navigation" spacecraft relative to the "truth" spacecraft prior to performing the maneuver. Cases 3-4 use the second apolune-to-apolune long-horizon maneuver option, while cases 5-6 use the first apolune-to-apolune option.*

Case	Long-Horizon Frequency [# of orbits]	3□ State Uncertainties [km, cm/s]	Mean Annual □V [m/s]	1□ □V [m/s]
1	10	N/A (8hr / day tracking)	4.273 +/- 2.061	2.061
2	15	N/A (8hr / day tracking)	4.050	2.093
3	10	10, 10	7.141	1.048
4	15	10, 10	6.856	1.169
5	10	10, 10	12.434	3.046
6	15	10, 10	11.51	2.50

Figures 9-11 show the results of a Monte Carlo analysis with 100 random trials for Case 1. The results shown here are for Gateway configuration #1 (PPE only, no crew). Figure 9 shows the stationkeeping maneuvers as performed. Note that most maneuvers are approximately 5-10 cm/s, but every 10 revolutions, a pair of larger maneuvers of approximately 50 cm/s each are performed. The small maneuvers are the short-horizon OMMs, and the large ΔVs correspond to the long-horizon maneuvers.

Figure 9. Stationkeeping maneuver magnitudes as performed.

Figure 10 shows the 1σ position and velocity covariance returned by a batch filter once per revolution at the data cutoff (24 hours before maneuver execution). The geometry and ground tracking for all the random trials is very similar, so the covariance results do not vary significantly from trial to trial. It is observed that following some of the long-horizon maneuvers, the state uncertainty is significantly larger than on the other revolutions. It is hypothesized that these come as a result of long-horizon maneuvers which happen to be aligned with the unstable eigenvector of the NRHO, but additional testing is required to understand the phenomena better. For the given tracking schedule, the state uncertainties are comparable to those found by past studies.

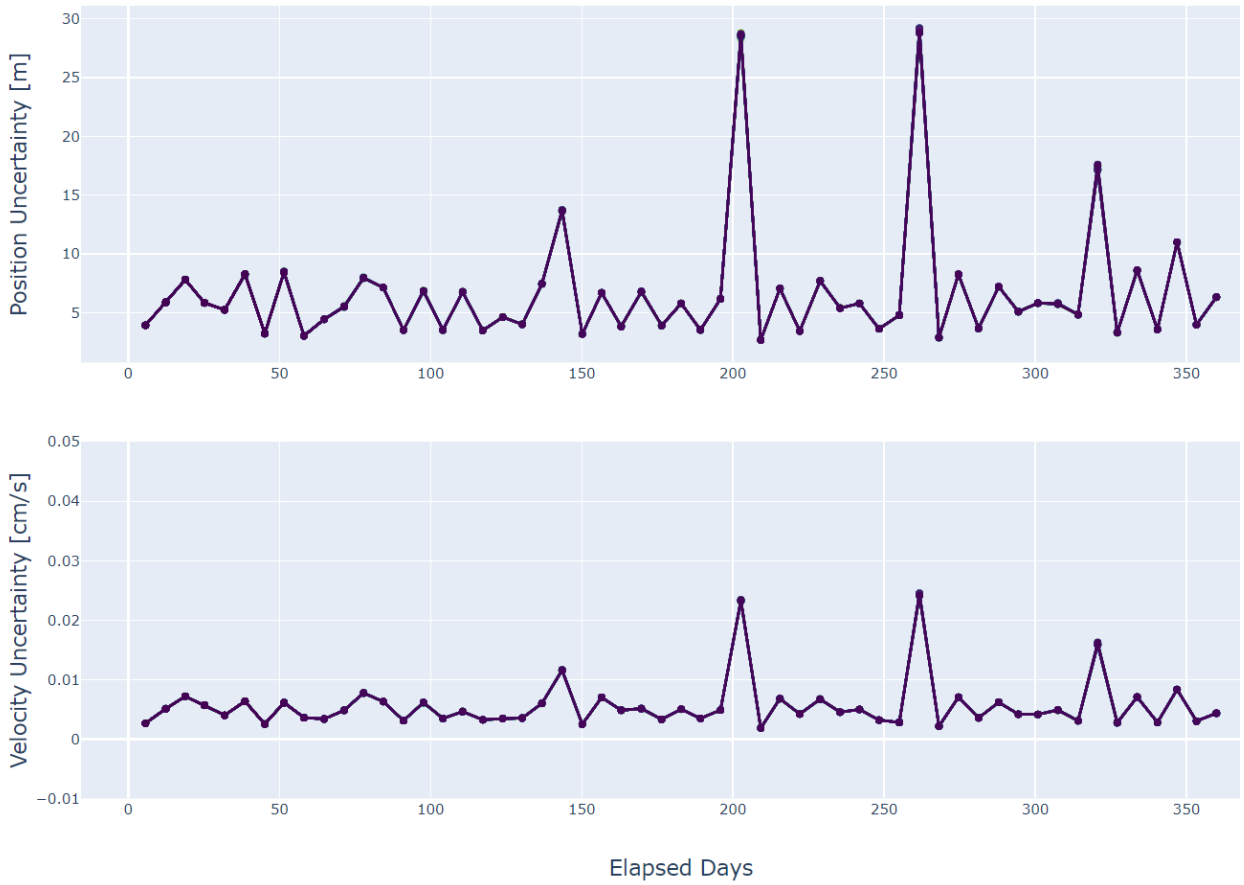

Figure 10. State uncertainty at each estimation epoch, with one eight-hour tracking pass per day.

Figure 11 shows the state error for each random trial immediately following each stationkeeping maneuver execution. The position errors are slightly larger than the uncertainties reported above, which is consistent with the uncertainty growing over the 24 hours between data cutoff and maneuver execution. The velocity error is substantially larger because of the ~3 cm/s desaturation maneuver performed immediately before the OMM and the OMM execution error.

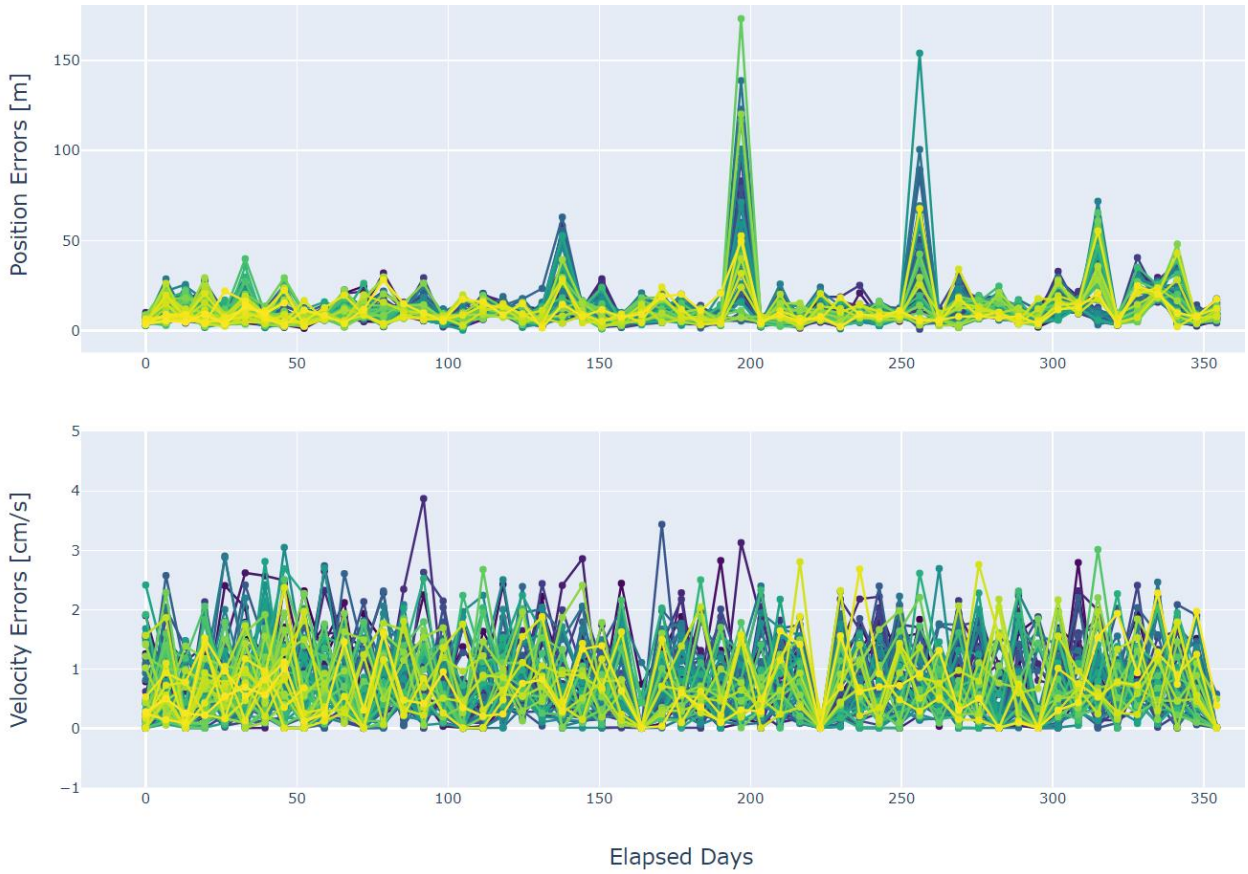

Figure 11. State error relative to truth immediately after each maneuver execution.

C. Navigation Trades

Several trades are presented to discuss the impact on navigation filter performance from tracking cadence, tracking pass phasing (where in the orbit the tracking passes take place), filter type, measurement noise, and measurement type.

Comparison of tracking cadence

For this analysis, a number of tracking cadences are evaluated with the U-D factorized covariance filter:

- Continuous
- 8 hours per pass, 7 passes per week
- 8 hours per pass, 3 passes per week
- 8 hours per pass, 2 passes per week
- 2 hours per pass, 7 passes per week
- 2 hours per pass, 3 passes per week
- 2 hours per pass, 2 passes per week

Table 8. Position and velocity 1-sigma uncertainties as a function of tracking cadence with U-D factorized covariance filter.

Tracking Cadence	Apolune Position Uncertainty [km]	Apolune Velocity Uncertainty [m/s]
Continuous	$1.41*10^{-2}$	$3.54*10^{-4}$
8 hours 7/week	$8.66*10^{-2}$	$8.04*10^{-4}$
8 hours 3/week	$4.17*10^{-1}$	$2.02*10^{-3}$
8 hours 2/week	$1.69*10^{-1}$	$4.42*10^{-3}$
2 hours 7/week	$1.48*10^{-1}$	$1.06*10^{-3}$
2 hours 3/week	$1.66*10^{-1}$	$1.14*10^{-3}$
2 hours 2/week	$1.69*10^{-1}$	$1.27*10^{-3}$

Interestingly, the "8 hours 3/week" case performs worse here than the "8 hours 2/week" case. This is because of where the tracking passes happen to fall in the orbit. For short data arcs like an NRHO revolution, the placement of tracking arcs with respect to the desired state can be more important than your cumulative tracking time.

Comparison of tracking pass phasing

A basic test to demonstrate the importance of where measurements are taken in the NRHO can be seen by analyzing the instantaneous uncertainty during a continuous tracking cadence. A plot showing this uncertainty is shown in Figure 14. The data arc begins at one apolune and ends at the next apolune, with perilune at approximately Aug-01-2024 12:00.

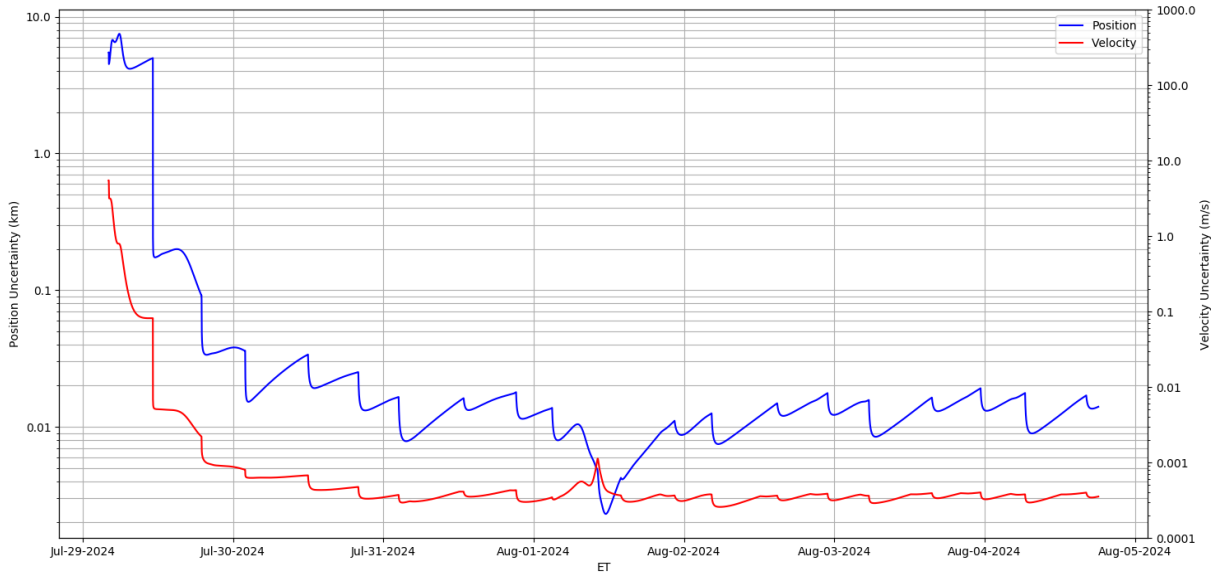

Figure 13. Position and velocity 1□ covariance magnitudes over one NRHO revolution with continuous tracking.

At perilune, the system is the most observable because the spacecraft traverses a large distance in a short time. As a result, the position covariance reaches its minimum at perilune. However, the difference between the gravity field used in the Truth and Navigation models becomes most apparent at perilune. The assumption that the dynamics are linearizable also breaks down the most at perilune. As a result of these effects, the velocity uncertainty is at a local

maximum at perilune. It is not immediately obvious whether the improved observability or the worsened linearizability has the greater net effect.

Additionally, despite continuous tracking through the entire orbit, a spike in velocity uncertainty still occurs as the spacecraft passes through perilune. The uncertainty spike in velocity at perilune highlights the sensitivity of the dynamics. A slight state error at apolune corresponds to a large error at perilune, and a slight state error at perilune corresponds to a large error at apolune.

Figures 14 shows the pre and post-filter Doppler residuals (in X-band Hz) of the simulated measurements.

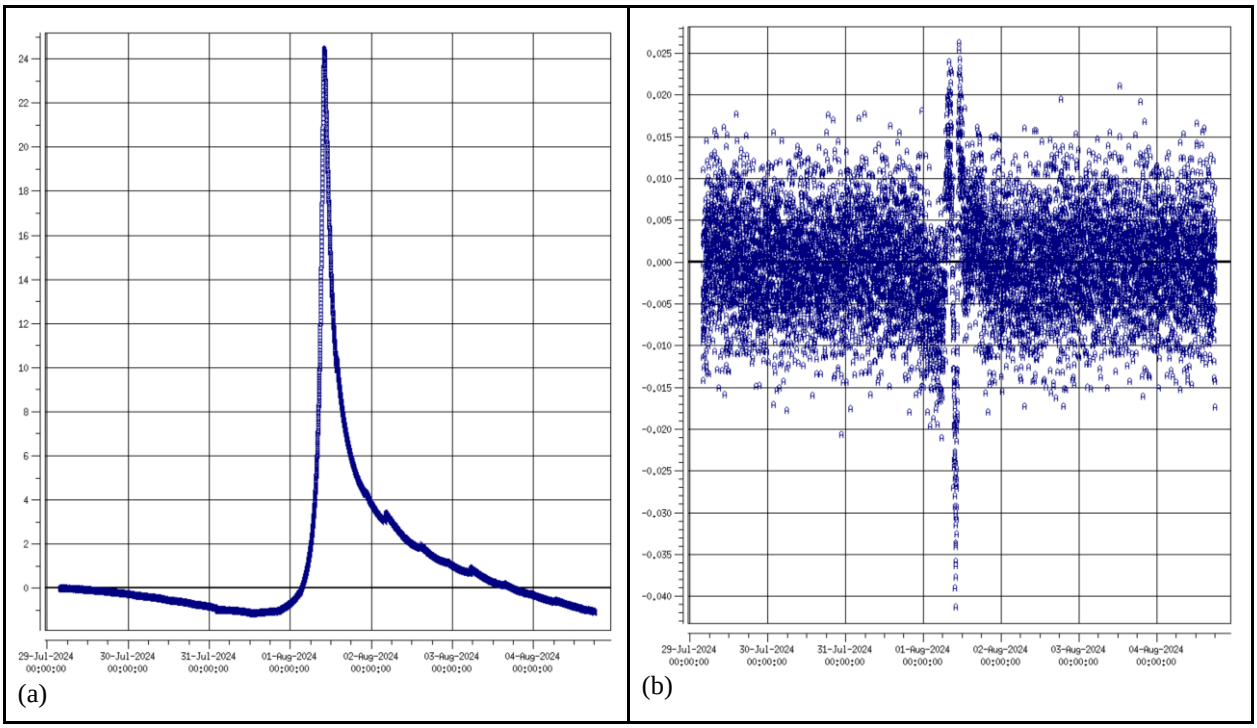

Figure 14. Prefit (a) and postfit (b) Doppler residuals (X-band Hz) over one NRHO revolution with continuous tracking.

Despite showing improvement over the a priori guess of the state, there are still clear artifacts of the chaotic dynamics at perilune, which leads to a spike in the velocity uncertainty. For this continuous tracking case, the spike is short lived, as new observations quickly correct the residuals. However, for cases where a tracking pass begins or ends at perilune, the filter may be thrown off by the fast dynamics.

Comparison of filter type

For this analysis, there are three tracking cadences used to compare the filter performance between GMAT and Monte. Each of the cadences uses a combination of three predefined tracking windows. The three tracking cadences are each 8 hours in duration, spaced about the NRHO in approximately-equal intervals. They are depicted in Figure 12. The first pass begins 1 day after apolune, the second pass begins 3 days after apolune, and the third pass begins 8 hours before DCO. The first analysis case uses only the first tracking pass, the second case uses the first pass and the third pass, and the third case uses all three passes. For each case considered, navigation was simulated for two years with 100 random samples.

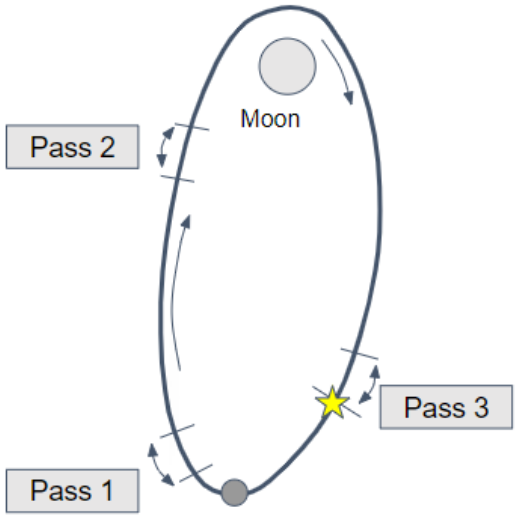

Figure 12. Three tracking windows used for comparison.

Table 9. Comparison of filter performance for different tracking cadences.

Measure of Performance	**Case**	**GMAT Batch**	**Monte U-D Factorized Covariance**	**Monte SRIF**
Mean covariance	1 pass per rev	TBD km, TBD cm/s	TBD km, TBD cm/s	TBD km, TBD cm/s
	2 passes per rev	TBD km, TBD cm/s	TBD km, TBD cm/s	TBD km, TBD cm/s
	3 passes per rev	TBD km, TBD cm/s	TBD km, TBD cm/s	TBD km, TBD cm/s
Mean accuracy relative to truth	1 pass per rev	TBD km, TBD cm/s	TBD km, TBD cm/s	TBD km, TBD cm/s
	2 passes per rev	TBD km, TBD cm/s	TBD km, TBD cm/s	TBD km, TBD cm/s
	3 passes per rev	TBD km, TBD cm/s	TBD km, TBD cm/s	TBD km, TBD cm/s
Filter convergence	1 pass per rev	0%	TBD	TBD
	2 passes per rev	50%	TBD	TBD
	3 passes per rev	90%	TBD	TBD

Comparison of measurement noise

In this analysis, the impact of measurement noise is considered for the case where three tracking passes are used per orbit, as described above. Filter performance is reported as covariance at the end of a representative data arc.

Table 10. Position and velocity 1-sigma uncertainties as a function of measurement noise with U-D factorized covariance filter.

Measurement noise	Apolune Position Uncertainty [km]	Apolune Velocity Uncertainty [m/s]
3 m, 1 mm/s	$4.17*10^{-1}$	$2.02*10^{-3}$
10 m, 10 mm/s	TBD	TBD
15 m, 25 mm/s	TBD	TBD

Comparison of measurement type

In this analysis, the impact of measurement type is considered for the case where three tracking passes are used per orbit, as described above. Range-only, range-rate-only, and range plus range-rate data types are considered with the U-D factorized covariance filter. Filter performance is reported as covariance at the end of a representative data arc.

Table 11. Position and velocity 1-sigma uncertainties as a function of measurement type with U-D factorized covariance filter.

Measurement type	Apolune Position Uncertainty [km]	Apolune Velocity Uncertainty [m/s]
Range only	TBD	TBD
Range-rate only	TBD	TBD
Range + range-rate	$4.17*10^{-1}$	$2.02*10^{-3}$

V. Conclusion

The analyses in this paper address a range of questions related to operating a spacecraft in an NRHO. Realistic requirements for tracking cadence, tracking measurement noise, and tracking pass phasing are derived from analysis. Popular filter types are compared to each other.

Future work will consider additional combinations of the various trades presented here. NASA and Advanced Space will demonstrate NRHO navigation and operation with the CAPSTONE mission, currently planned for launch in December 2020.

The authors wish to acknowledge support from the NASA SBIR (Small Business Innovative Research) program, and Caltech for the use of Monte software.